J Math Chem (2009) 45:452–459
DOI 10.1007/s10910-008-9418-z

ORIGINAL PAPER

Elongated tori from armchair DWNT

Csaba L. Nagy · Katalin Nagy · Mircea V. Diudea

Published online: 9 August 2008
© Springer Science+Business Media, LLC 2008

Abstract The structure and stability of axially elongated carbon tori obtained by connecting the adjacent walls of an armchair DWCNT is studied. Two types of junctions are considered, convertible by Stone-Wales isomerisation. The energy of the structure with respect to the length difference of the tubes is investigated with PM3 semiempirical method.

Keywords DWCNT · Elongated torus · Junction · Fusion · Semiempirical

1 Introduction

Circular polyhex tori [1,2] can be obtained by uniform bending and connection of its two ends of a sufficiently long single-walled carbon nanotube. These tori can form stable structures only beyond a critical radius [3–6], when the strain energy introduced by bending the tube is smaller then the energy gain by the formation of covalent bonds of the open nanotube. A simple estimate shows [3] that the critical radius of an elastic torus made from a (10,10) nanotube is approximately 90 nm. Large scale molecular dynamics simulation [4] indicates that the strain energy is evenly distributed over each atom if the cross section of the torus is also circular. Notice that large number of atoms is required in order to form a stable polyhex torus.

Junctions between two nanotubes with different chirality can be realized by introducing a pentagon–heptagon pair, termed Dunlap knee [7]. By the periodical repetition of these connections, seamless tori can be generated with small curvature radius [8–11]. The resulting tori would be polygonal if the number of defects is small.

C. L. Nagy (✉) · K. Nagy · M. V. Diudea
Faculty of Chemistry and Chemical Engineering, Babeş-Bolyai University,
Arany J. Str 11, 400028 Cluj-Napoca, Romania
e-mail: nc35@chem.ubbcluj.ro

Polygonal tori can be given a more circular appearance by incorporation of a sufficient number of nonhexagonal rings.

This work presents toroidal structures obtained by connecting the walls of a DWCNT at both ends. There are several examples when carbon structures coalesce under different condition, like electron irradiation or thermal annealing. Diameter doubling [12] of parallel single-walled armchair nanotubes with identical chirality has been observed. Using electron irradiation treatments of C_{60}@SWCNT the C_{60} molecules start to coalesce, producing nanocapsules inside the tubes [13,14]. It is proposed that the linking of concentric nanotubes could be possible by creating defects in the carbon network.

Hemitoroidal nanotube tip structures have been produced by passage of an arc between graphite rods [15,16]. These structures appear to form as a result of optimal graphitization of two or more adjacent concentric graphene tubules.

2 Torus construction

To achieve closure of adjacent concentric walls of a double-walled nanotube, bonds must be broken and new ones to be made, such that a completely trivalent sp^2 junction (with no defects) results at both ends of the DWCNT. With the elimination of dangling bonds this process leads to the formation of an axially elongated torus. Consider an armchair DWCNT with an outer tube of twice the diameter as the inner one, i.e. (10,10)(5,5). In Fig. 1 the planar projection of a segment of the model is presented. The upper large and lower small hexagons represent the inner and outer nanotube, respectively. By breaking the bonds marked in boldface and connecting the resulted dangling atoms with two atoms from the outer tube (dotted bonds) a complete trivalent junction arise.

The walls of the DWCNT are linked by a sequence of non-hexagonal units (section between square brackets in Fig. 1, an octagon adjacent with two pentagons, separated by a hexagon. By the Stone-Wales transformation [17] of the bonds connecting the two pentagons, the unit is transformed into a pentagon–heptagon pair. Hereafter these structures will be labeled *pop* and *ph* tori, respectively, according to the sequence of non-hexagonal faces comprised in he junction.

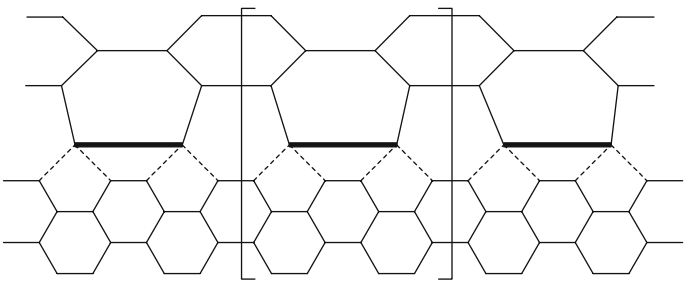

Fig. 1 Connection of the walls of a DWCNT

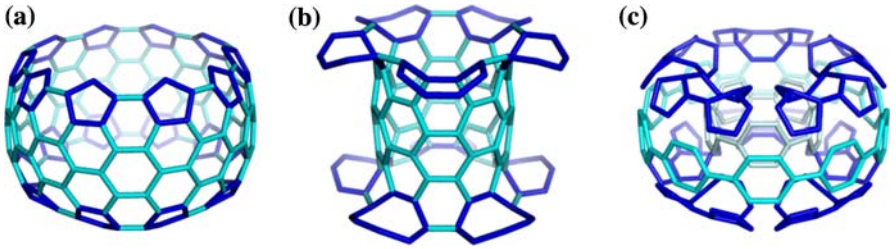

Fig. 2 The elements of a *pop*-torus (junction in dark color). (**a**) *pop*-(10, 10, 7)-outer, (**b**) *pop*-(5, 5, 10)-inner, (**c**) parts of *pop* torus

As it was mentioned in Sect. 1, pentagons and heptagons provide positive and negative Gaussian curvature, respectively. Therefore, pentagons are located on the outermost region of the torus, while octagons are present in the inner surface (i.e. the torus hollow). Figure 2 presents the outer (a) and inner (b) surface of a *pop* torus, where the non-hexagonal faces are marked in dark color. The structure can be divided in four segments: two polyhex tubular sections and two junctions with non-hexagonal faces (see Fig. 2c).

According to the generalized Euler's law, only genus one structures can be tiled exclusively with hexagons, for instance polyhex nanotubes and nanotori [1]. The number of non-hexagonal faces (i.e. pentagons and heptagons) that are necessary to be introduced in the hexagonal network to result a polygonal torus, can be calculated from Euler's formula. In the case of a *pop* torus the number of pentagons is twice the number of octagons, $f_5 = 2 \cdot f_8$, while in the case of a *ph* torus there are equal number of pentagons and heptagons, $f_5 = f_7$.

2.1 Torus notation

The structures were labeled according to the junction type (*pop* or *ph*), the chirality and size of both outer ($m_\mathrm{o}, n_\mathrm{o}, l_\mathrm{o}$) and inner ($m_\mathrm{i}, n_\mathrm{i}, l_\mathrm{i}$) nanotubes, and the point group symmetry (D_{5h}, D_{5d}, D_5).

Three parameters (*m*,*n*,*l*) were used for the notation of the nanotubes, where the first two represents the lattice translational indices *m* and *n*. Since only armchair tubes are considered, *m* and *n* are equal. To count the length of the nanotube a third parameter *l* was introduced, which in case of armchair nanotubes it corresponds to the half of the unit cell. According to this notation the (10,10,2) nanotube is actually the unit cell of the (10,10) armchair nanotube. Considering that the values of *l* could be even or odd, the symmetry of the torus depends on the length of the outer (l_o) and inner (l_i) nanotube:

- if both l_o and l_i are odd, the torus has D_{nh} symmetry;
- if l_o is odd and l_i is even, the torus has D_{nd} symmetry;
- if l_o is even and l_i is odd, or both l_o and l_i are even, the torus has D_n symmetry.

The principal symmetry axe is defined by the number of *pop* or *ph* units in the junction zone. It is also determined by the chirality of the tubes ($m_\mathrm{o}/2 = m_\mathrm{i}$-fold).

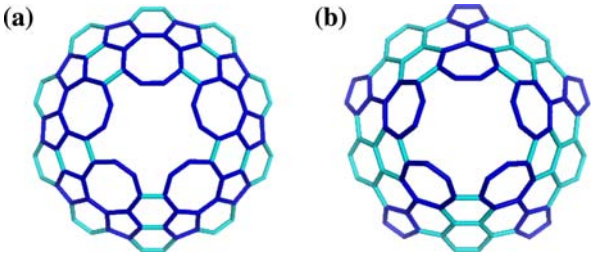

Fig. 3 The junction comprises of five number of *pop* or *ph* units, respectively. (**a**) *pop*-(10,10)(5,5)-junction, (**b**) *ph*-(10,10)(5,5)-junction

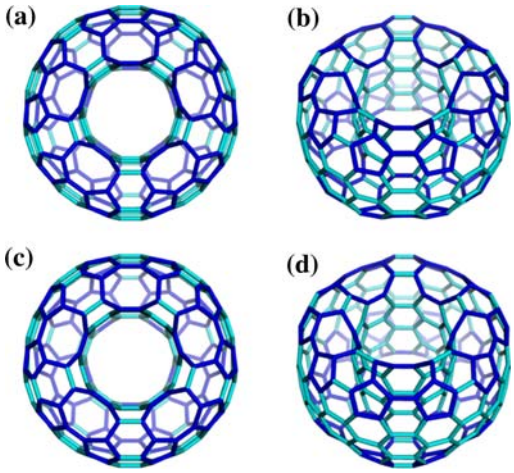

Fig. 4 Example of *pop*-torus with D_{5h} and D_{5d} symmetry. (**a**) *pop*-(10,10,7)(5,5,9)-D_{5h} top view, (**b**) *pop*-(10,10,7)(5,5,9)-D_{5h} side view, (**c**) *pop*-(10,10,7)(5,5,10)-D_{5d} top view, (**d**) *pop*-(10,10,7)(5,5,10)-D_{5d} side view

All structures studied herein have a fivefold symmetry axe owing to the five *pop* units (Fig. 3a) and five *ph* units (Fig. 3b) respectively.

2.2 pop torus

For the construction of our series of tori, the length of the outer nanotube remained constant, i.e. (10,10,7), while the length of the inner wall of the DWNT was increased from $l_{\mathrm{i}} = 4$ to 14. At length of the inner tube $l_{\mathrm{i}} = 4$ an octagon shares two edges with two octagons from the opposite side. At length $l_{\mathrm{i}} = 5$ two octagons from opposite sides have one common bond, and with the further increase of the tube length they are at $(l_{\mathrm{i}} - 5)$ bond distance.

Two *pop* tori with D_{5h} (Fig. 4a and b) and D_{5d} (Fig. 4c and d) symmetry are presented in both top and side view. It can be seen that *pop* units (marked in darked color) are superimposed in the case of the torus with D_{5h} symmetry, while in the other case they are staggered. Notice that the position of the junction changes with the increase of the inner tube.

2.3 ph torus

The structures resulted by Stone-Wales transformation of the *pop* units, through the rotation of the bond connecting the two pentagons. The symmetry is preserved but the

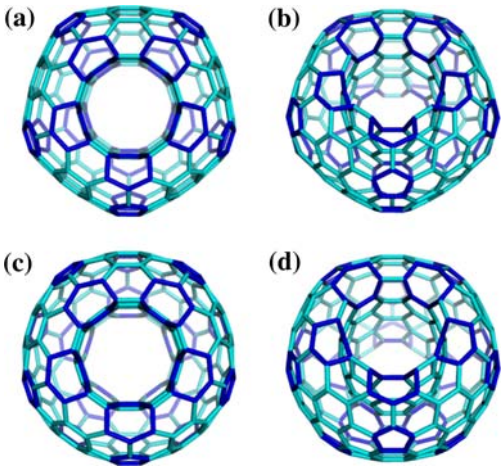

Fig. 5 Example of *ph*-torus with D_{5h} and D_{5d} symmetry. **a**) *ph*-(10,10,7)(5,5,9)-D_{5h} top view, (**b**) *ph*-(10,10,7)(5,5,9)-D_{5h} side view, (**c**) *ph*-(10,10,7)(5,5,10)-D_{5d} top view, (**d**) *ph*-(10,10,7)(5,5,10)-D_{5d} side view

structure has a polygonal shape, as viewed along the fivefold axis. Figure 5 presents the transformed tori corresponding to the structures from Fig. 4.

3 Results and discussion

The energetics and equilibrium geometries of both elongated tori were obtained using the PM3 semiempirical potential. To study the stability change within the *pop* and *ph* torus series, three parameters were followed: the variation of the heat of formation and HOMO-LUMO energy gap resulted from PM3 semiempirical computations, and the strain (both global and local) of the structures calculated according to the POAV theory [18].

Figure 6 presents the variation of the heat of formation per atom plotted against the length of the inner nanotube. The energy curve with circles represents the values for the *pop* tori, while the one with triangles corresponds to the *ph* tori.

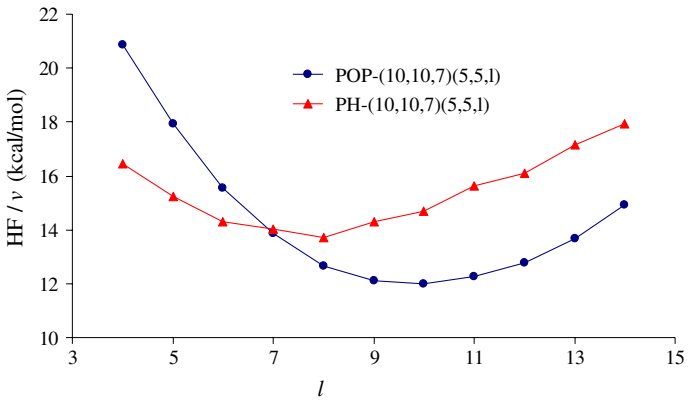

Fig. 6 Variation of heat of formation as a function of inner tube length

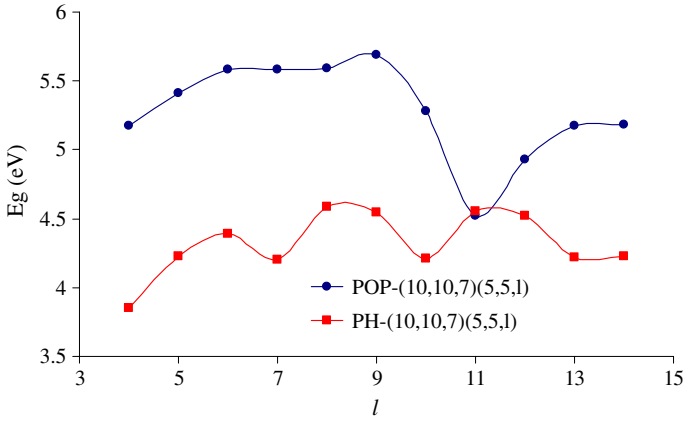

Fig. 7 Variation of heat of HOMO-LUMO energy gap as a function of inner tube length

The stability of the torus mainly depends on the relative position of the junction zone. In the smallest structure with $l = 4$ every octagon shares two edges with other two octagons from the opposite side, and all of them are located in the middle of the torus hollow. The octagons are pushed towards the nanotube tips and the stability of the torus increases accordingly, as the length of the inner tube increases. Beyond a certain limit of the inner tube length relative to the outer one, the energy of the torus will increase, owing to octagons that are displaced on the outer section. Consequently *pop*-(10,10,7)(5,5,16)-D_{5d} torus could not be optimized due to large strain.

The torus with the smallest energy per atom is *pop*-(10,10,7)(5,5,10)-D_{5d}, however the structures with the length of the inner tube $l = 8$–11 are in the same stability range.

In the same fashion the energy of the *ph* tori depends on the placement of the pentagons and heptagons. Notice that while in the case of *pop* torus the pentagons are adjacent to the octagon, here the pentagon is at one bond distance from the heptagon. Consequently the *ph* torus with minimal energy per atom will not correspond to that of the *pop* one, because of the pentagon that is pushed away from the nanotube tips towards the outer tube.

The HOMO-LUMO gap energy variation is presented in Fig. 7, where the curves are labeled in compliance with those in Fig. 6. A periodicity of three can be observed in the variation of the energy gap of the *ph*-tori, similar to the case of capped armchair nanotubes [19,20].

It is obvious that the strain is not evenly distributed over all the atoms, thus the strain energy per atom is not sufficient for identification of the energetic stability of these carbon structures. Therefore to find the contribution of different segments of the molecule to the global strain, the torus was divided into four parts.

Local strain calculations of the molecule segments are presented in Fig. 8, where the strain of both the inner (empty triangles) and outer (empty circles) tubular section (the sum of them is also given), and that of the junctions (triangles) are represented versus m. For comparison the overall strain is presented. Since the strain of both junctions is equal, only one energy curve is presented. Notice that after separating the junctions,

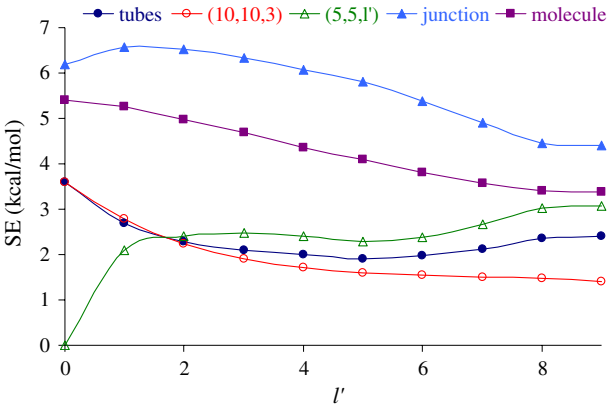

Fig. 8 Strain energy variation of different segments of the torus with the inner tube length

the size of the outer tube in every structures is (10,10,3), while the inner tube is (5,5,l') where $l' = (l - 6)$, hence it is 0 for $l = 4 - 6$.

The strain of the molecules shows a linear decrease with respect to the length of the inner tube. However the strain of the inner tube segment is in compliance with the heat of formation variation.

4 Conclusions

The structure and energy of axially elongated tori obtained by the closure of the adjacent walls of a double-walled carbon nanotube have been discussed. Two types of junctions were considered, *pop*- and *ph*-tori, the structures were labeled according to the size of faces within the junction. The obtained results demonstrate that the stability of the torus depends on the difference in the length of the tubes. *ph*-tori are preferred over the *pop*-tori if the length of the inner tube is smaller than the outer one than. Still the *pop*-tori are more stable at equal tube lengths and in the case with a longer inner tube.

References

1. E.C. Kirby, Croat. Chem. Acta **66**, 13–26 (1993)
2. E.C. Kirby, R.B. Mallion, P. Pollak, J. Chem. Soc. Faraday Trans. **89**, 1945–1953 (1993)
3. V. Meunier, P. Lambin, A.A. Lucas, Phys. Rev. B **57**, 14886–14890 (1998)
4. J. Han, Chem. Phys. Lett. **282**, 187–191 (1998)
5. M. Huhtala, A. Kuronen, K. Kaski, Comput. Phys. Commun. **146**, 30–37 (2002)
6. M. Huhtala, A. Kuronen, K. Kaski, Comput. Phys. Commun. **147**, 91–96 (2002)
7. B.I. Dunlap, Phys. Rev. B **46**, 1933–1936 (1992)
8. S. Ihara, S. Itoh, J.-I. Kitakami, Phys. Rev. B **47**, 12908–12911 (1993)
9. S. Ihara, S. Itoh, J.-I. Kitakami, Phys. Rev. B **48**, 5643–5647 (1993)
10. S. Itoh, S. Ihara, Phys. Rev. B **47**, 1703–1704 (1993)
11. S. Itoh, S. Ihara, Phys. Rev. B **48**, 8323–8328 (1993)
12. P. Nikolaev, A. Thess, A.G. Rinzler, D.T. Colbert, R.E. Smalley, Chem. Phys. Lett. **266**, 422–426 (1997)

13. S. Bandow, T. Hiraoka, T. Yumura, K. Hirahara, H. Shinohara, S. Iijima, Chem. Phys. Lett. **394**, 320–325 (2004)
14. T. Yumura, K. Hirahara, S. Bandow, K. Yoshizawa, S. Iijima, Chem. Phys. Lett. **386**, 38–43 (2004)
15. M. Endo, K. Takeuchi, K. Kobori, K. Takahashi, H.W. Kroto, A. Sarkar, Carbon **33**, 873–881 (1995)
16. A. Sarkar, H.W. Kroto, M. Endo, Carbon **33**, 51–55 (1995)
17. A.J. Stone, D.J. Wales, Chem. Phys. Lett. **128**, 501–503 (1986)
18. R.C. Haddon, J. Am. Chem. Soc. **119**, 1797–1798 (1997)
19. R. Saito, M. Fujita, G. Dresselhaus, M.S. Dresselhaus, Phys. Rev. B **46**, 1804–1811 (1992)
20. J. Li, Y. Zhang, M. Zhang, Chem. Phys. Lett. **364**, 338–344 (2002)